



Contents lists available at ScienceDirect



## Catalysis Today

journal homepage: [www.elsevier.com/locate/cattod](http://www.elsevier.com/locate/cattod)

# Selective conversion of microcrystalline cellulose into hexitols over a Ru/[Bmim]<sub>3</sub>PW<sub>12</sub>O<sub>40</sub> catalyst under mild conditions

Xianna Xie<sup>a</sup>, Jinyu Han<sup>a</sup>, Hua Wang<sup>a,\*</sup>, Xinli Zhu<sup>a</sup>, Xiao Liu<sup>a</sup>, Yufei Niu<sup>a</sup>, Zhiqiang Song<sup>a</sup>, Qingfeng Ge<sup>a,b,\*\*</sup>

<sup>a</sup> Key Laboratory for Green Chemical Technology of State Education Ministry, School of Chemical Engineering & Technology, Tianjin University, Tianjin 300072, PR China

<sup>b</sup> Department of Chemistry and Biochemistry, Southern Illinois University, Carbondale, IL 62901, USA

## ARTICLE INFO

## Article history:

Received 1 August 2013

Received in revised form

23 September 2013

Accepted 26 September 2013

Available online xxx

## Keywords:

Ru/[Bmim]<sub>3</sub>PW<sub>12</sub>O<sub>40</sub>

Celllobiose and cellulose

Hydrogenolysis

Hydrogen spillover

Brønsted acid

## ABSTRACT

A catalyst consisting of dispersed Ru on an ionic liquid (BmimPF<sub>6</sub>)–heteropolyacid (H<sub>3</sub>PW<sub>12</sub>O<sub>40</sub>·nH<sub>2</sub>O) hybrid as a support, i.e. Ru/[Bmim]<sub>3</sub>PW<sub>12</sub>O<sub>40</sub>, has been successfully synthesized. The catalyst, which combines the Ru sites for hydrogenation and both Lewis and Brønsted acidic sites for hydrolysis, exhibits a superior catalytic performance for selective conversion of the microcrystalline cellulose to hexitols over the catalyst of mixing [Bmim]<sub>3</sub>PW<sub>12</sub>O<sub>40</sub> and Ru/C. On the Ru/[Bmim]<sub>3</sub>PW<sub>12</sub>O<sub>40</sub> catalyst, a sorbitol selectivity of 70.3% with a microcrystalline cellulose conversion of 63.7% was achieved in 24 h at 433 K and 5 MPa H<sub>2</sub>. The superior catalytic performance of Ru/[Bmim]<sub>3</sub>PW<sub>12</sub>O<sub>40</sub> has been characterized using the hydrogenolysis of celllobiose as a probe reaction and was attributed to the Brønsted acid sites generated from hydrogen spillover from the Ru sites to the O sites of the support. In situ generation of the Brønsted acidic sites through hydrogen spillover has been confirmed by FT-IR characterization of pyridine adsorption. Furthermore, pH changes after treating the catalyst in H<sub>2</sub> demonstrated that dissolution of the protons generated on the oxygen sites as a result of hydrogen spillover acidifies the liquid product. These Brønsted acids work synergistically with the supported Ru and contribute to the enhanced hydrogenolysis activity.

© 2013 Elsevier B.V. All rights reserved.

## 1. Introduction

Selective conversion of renewable lignocellulosic biomasses, such as cellulose, to low molecular alcohols and/or hydrocarbons is crucial to a wide spread use of the most abundant, inexpensive and renewable sources [1]. Producing commodity chemicals or fuels from biomass-based resources will reduce the reliance on fossil resources and help to improve a nation's energy security [2–8]. However, the strong β-1,4-glycosidic bond in cellulose as well as intra- and inter-molecular hydrogen bonds result in a robust crystalline structure, which made the hydrogenolysis of cellulose under mild conditions a great challenge [9].

Mixed catalysts that combine active sites for hydrolysis and hydrogenation are attractive for cellulose conversion [10–12]. Palkovits and coworkers demonstrated a yield of ~81% toward C4 to C6 sugar alcohols (C6 53.0%, C5 8.9%, C4 18.7%) at 433 K and 5 MPa H<sub>2</sub> in 7 h over a combined H<sub>4</sub>SiW<sub>12</sub>O<sub>40</sub>–Ru/C catalyst in the

conversion of cellulose [13]. On the other hand, Geboers et al. reported a 49% hexitols yield (sugar alcohol 32%, sorbitan 17%) with a conversion of 82% over the H<sub>4</sub>SiW<sub>12</sub>O<sub>40</sub>–Ru/C catalyst at 463 K and 5 MPa H<sub>2</sub> in 24 h [14]. The same group performed an one-step conversion of ball-milled cellulose over a catalyst mixing the cesium salts of HPAs calcined at 600 °C and Ru/C, yielding a 90% hexitols (alditol 70%, sorbitan 20%) with a 100% conversion after 48 h [15]. In those catalysts, Ru, the active sites for hydrogenation, is supported on C and not in direct contact with the acidic sites of the ployacids, which are active for hydrolysis. Liu et al. reported briefly a study on the conversion of ball-milled cellulose over the catalysts prepared by loading Ru nanoparticles directly on the Cs salts of H<sub>3</sub>PW<sub>12</sub>O<sub>40</sub> [16]. The authors showed that a sorbitol yield of 43% at 433 K after 24 h reaction can be achieved over the Ru/Cs<sub>3</sub>PW<sub>12</sub>O<sub>40</sub> catalyst and suggested that the Brønsted acid sites generated in situ through hydrogen spillover [17–19] made up for the missing intrinsic Brønsted acidity and contributed to the observed enhancement of catalytic performance.

Ionic liquids (ILs) are a class of non-volatile green solvents and have been studied extensively for dissolution of cellulose [20]. The IL–HPA hybrids are more stable, and less sensitive to humidity and temperature than the parent HPAs [21] and have been reported to exhibit excellent performance in electrochemistry

\* Corresponding author.

\*\* Corresponding author at: Department of Chemistry and Biochemistry, Southern Illinois University, Carbondale, IL 62901, USA. Tel.: +1 618 4536406.

E-mail addresses: [tjuwanghua@tju.edu.cn](mailto:tjuwanghua@tju.edu.cn) (H. Wang), [qge@chem.siu.edu](mailto:qge@chem.siu.edu) (Q. Ge).

and catalysis [22–27] due to their superior proton conductivity. In order to enhance the acidity of the IL–HPA hybrids, several authors attempted to incorporate acidic functional groups into the organic cations. For example, Dyson and Kou's group used the catalytic system composed of metal NPs and a functionalized Brønsted acidic IL immobilized in a nonfunctionalized IL, allowing hydrogenation and dehydration reactions to occur in tandem [28]. Huang et al. showed that sulfonated IL–HPA salts ( $[MIMPSH]_n H_{3-n} PW_{12}O_{40}$  ( $n=1, 2, 3$ )) were able to dehydrate fructose into 5-hydroxymethyl furfural (5-HMF) [29]. The same catalyst showed a glucose yield of 36% for cellulose hydrolysis at 413 K in 5 h with water and methyl isobutyl ketone (MIBK) as solvents [30]. However,  $[MIMPSH]_n H_{3-n} PW_{12}O_{40}$  are soluble in water, which makes the recovery of the catalyst a challenge. Therefore, an insoluble IL–HPA hybrid would be an ideal support for a Ru hydrogenation catalyst for the selective conversion of cellulose.

In the present study, we successfully dispersed Ru on an insoluble hybrid material of  $IL(BmimPF_6)-HPA(H_3PW_{12}O_{40}\cdot nH_2O)$ . The catalyst has been demonstrated to have a high selectivity toward sorbitol for the hydrogenation/hydrolysis of microcrystalline cellulose in a one-pot process. Our characterization showed that the Ru/IL–HPA catalyst generates Brønsted acidic sites in situ and acidifies the liquid reactive mixture. On this catalyst, the active sites for hydrogenation and hydrolysis coexist and work synergistically.

## 2. Experimental details

### 2.1. Materials

Microcrystalline cellulose from Sigma-Aldrich, cellobiose (98%) from Acros, 12-phosphotungstic acid (AR) from Kermel (Tianjin, China), activated carbon-supported Ru (5 wt% Ru) from Dalian Tongyonger Chemical Co. Ltd., and 1-butyl-3-methylimidazolium hexafluorophosphonate ( $[Bmim]PF_6$ ) from Henan Lihua Pharmaceutical Co., Ltd were used as received without further purification. Standard chemicals including glucose, sorbitol, anhydrous sorbitol, xylitol, erythritol and others were purchased from Sigma-Aldrich.

### 2.2. Catalyst preparation

#### 2.2.1. Synthesis of $[Bmim]_3PW_{12}O_{40}$

$[Bmim]_3PW_{12}O_{40}$  was prepared by following the procedure reported by Ammam and Fransaer [23]. In a typical preparation, adding  $[Bmim]PF_6$  (6 mmol) directly to a  $H_3PW_{12}O_{40}$  solution prepared by dissolving 2 mmol  $H_3PW_{12}O_{40}$  in deionized water (10 mL) at room temperature and stirring the mixture for 24 h results in precipitates. The precipitates were filtered, then washed with deionized water and dried in vacuum, resulting in the solid product. The product has been characterized as  $[Bmim]_3PW_{12}O_{40}$ .

#### 2.2.2. Synthesis of Ru/ $[Bmim]_3PW_{12}O_{40}$

Ru/ $[Bmim]_3PW_{12}O_{40}$  was prepared with a conventional impregnation method: a mixture of solid  $[Bmim]_3PW_{12}O_{40}$  (2 g) and  $RuCl_3$  (0.2632 g) in 10 mL ethanol solution was stirred for 24 h at room temperature, followed by drying at 353 K overnight. The resulting solid was reduced in  $H_2$  at 473 K for 3 h, corresponding to 5 wt% Ru on the support, before being used as a catalyst in subsequent reactions. The catalyst was denoted as Ru/ $[Bmim]_3PW_{12}O_{40}$ .

### 2.3. Reaction procedures

The one-pot conversion of cellobiose and microcrystalline cellulose into hexitols was conducted in a lab-scale batch reactor with a Teflon insert (20 mL) heated in an oil bath and stirred by an electromagnetic stick. In a typical catalytic reaction run, 0.25 g microcrystalline cellulose or cellobiose, 0.05 g catalyst and 5 mL

deionized water were added to the reactor. The reactor was then flushed with hydrogen to 5 MPa and heated to the desired reaction temperature (measured in the Teflon insert). After reaction, the reactor was quickly cooled in an ice bath. The solid residual containing the catalyst and unreacted cellulose were separated from the liquid product using centrifugation. The liquid products were quantified using HPLC equipped with a refractive index detector and ICsep Coregel-87H column. An aqueous solution of  $H_2SO_4$  at 0.005 M with a flow rate of 0.6 mL/min was used as the mobile phase. A series of calibration standards with different concentrations have been prepared and measured with the same column on the HPLC. By comparing the retention time and peak area of the sample with that of the calibration standards under the same condition, a particular component of the liquid products corresponding to each peak can be determined. The amount of the product can be quantified with the peak area by referring to the standard curve. The HPLC column used in the present study can identify and quantify soluble saccharides (sucrose, fructose, xylose, etc.), C1–C6 alcohol (methanol, propanediol, sorbitol, etc.), carboxylic acids (lactic acid, levulinic acid, formic acid, etc.), carbonyls (formaldehyde, acetaldehyde) and some other small organic molecules. The solid residual containing the catalyst and the unreacted cellulose were dried overnight before being weighed.

The conversion of cellulose was calculated as the ratio of the weight difference between the solids before and after reaction to the initial weight of cellulose. The conversion of cellobiose was determined from the HPLC standard curve. The yield and selectivity of a specific product were calculated as: yield (%) = [moles C in product/total moles C loaded in reactor] × 100%; selectivity (%) = yield/conversion × 100% [31].

## 3. Results and discussion

### 3.1. Characterization of catalyst

The C, H and N contents were determined with a Vario MICRO cube elemental analyzer and the W and P contents were measured using an inductively coupled plasma emission (ICP; ICP-9000, USA Thermo Jarrell-Ash Corp) spectrometry. The sample was treated at 200 °C in a  $N_2$  stream for 3 h prior to elemental analysis. The results showed that the C, N, H, P and W contents in the catalyst are 8.90%, 2.53%, 1.52%, 0.96% and 65.82%, respectively. The theoretical values calculated based on the molecular formula,  $[Bmim]_3PW_{12}O_{40}$ , are 8.74% for C, 2.55% for N, 1.37% for H, 0.94% for P and 66.98% for W. Apart from H, the elemental analysis and ICP results showed that the elemental ratio is within 2% of the  $[Bmim]_3PW_{12}O_{40}$  formula value. Therefore, the as-synthesized compound is denoted as  $[Bmim]_3PW_{12}O_{40}$ . TG analysis showed that the synthesized  $[Bmim]_3PW_{12}O_{40}$  is stable up to 673 K. Obvious decomposition occurs at 723 K, as shown in Fig. S1 of the Electronic Supplementary Information.

The SEM and TEM analysis have been used to monitor the morphology and dispersion of the support and catalysts and the images (Figs. S2 and S3) are provided in the Electronic Supplementary Information. SEM images show that the crystallines of  $[Bmim]_3PW_{12}O_{40}$  are in the form of block-shaped particles. The particle sizes range from several hundred nanometers to a few microns. In contrast, TEM images show that Ru is dispersed uniformly on the support and its particles in the Ru/ $[Bmim]_3PW_{12}O_{40}$  sample are uniform spherical nanoparticles with a size of 4–5 nm.

The XRD patterns of (a)  $H_3PW_{12}O_{40}-nH_2O$ , (b)  $[Bmim]_3PW_{12}O_{40}$ , and (c) Ru/ $[Bmim]_3PW_{12}O_{40}$  are shown in Fig. 1. Long-range order was clearly shown in these XRD patterns. In addition, the diffraction peaks of (b) and (c) is different from that of (a) due to the substitution of the protons in  $H_3PW_{12}O_{40}-nH_2O$  by

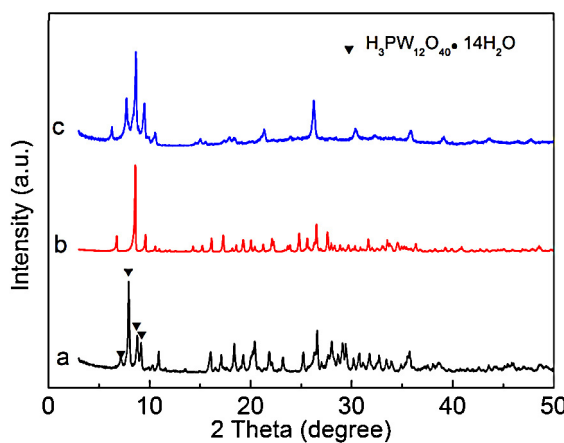


**Fig. 1.** XRD patterns of (a)  $\text{H}_3\text{PW}_{12}\text{O}_{40}$ , (b)  $[\text{Bmim}]_3\text{PW}_{12}\text{O}_{40}$ , and (c)  $\text{Ru}/[\text{Bmim}]_3\text{PW}_{12}\text{O}_{40}$ .

$[\text{Bmim}]^+$  in  $[\text{Bmim}]_3\text{PW}_{12}\text{O}_{40}$ . This is because that the crystalline structure was formed from packing the anions of the heteropolyacids, with the  $[\text{Bmim}]^+$  filling the interstitials. Therefore, the diffraction peaks in 5–10° should be results from the low-index planes of the crystalline packing as the lattice parameters are typically larger than 10 Å. The peaks in the 2 theta range of 10–40° should be diffraction from higher index planes. As W is a good X-ray scatter, long rang order originated from W in the crystal are expected to contribute to the observed diffraction peaks in this range. These XRD patterns show that the arrangement of the heteropolyacid cages remains to be the dominant feature of the hybrid with the ionic liquid as well as the  $\text{Ru}/[\text{Bmim}]_3\text{PW}_{12}\text{O}_{40}$  sample. The main diffraction peak of metallic Ru corresponding to the (110) planes should appear at 2 theta of ~44°, corresponding to the weak feature in Fig. 1(c). As the Ru particles are small, ~4–5 nm according to TEM micrograph, the diffraction peaks are expected to be weak and broad. Furthermore, there also peaks originating from  $[\text{Bmim}]_3\text{PW}_{12}\text{O}_{40}$  and  $\text{H}_3\text{PW}_{12}\text{O}_{40}$  around this angle, making the unambiguous assignment of the diffraction peak difficult.

Fourier transform infrared (FTIR) analysis was performed under vacuum on the Nicolet6700 spectrometer (KBr method). The FTIR spectra of the samples are collected in Fig. 2. As shown in Fig. 2, bulk  $\text{H}_3\text{PW}_{12}\text{O}_{40}$  shows characteristic bands associated with the Keggin unit, i.e. the P–O band at 1079 cm<sup>-1</sup>, the W–O band at 981 cm<sup>-1</sup>, the W–O–W bands at 893 cm<sup>-1</sup> and 798 cm<sup>-1</sup>, and a weak W–O–P band at 520 cm<sup>-1</sup> [32]. The characteristic bands of the Keggin unit can also be observed in the  $[\text{Bmim}]_3\text{PW}_{12}\text{O}_{40}$ ,  $\text{RuCl}_3/[\text{Bmim}]_3\text{PW}_{12}\text{O}_{40}$  and  $\text{Ru}/[\text{Bmim}]_3\text{PW}_{12}\text{O}_{40}$  samples, indicating the cage structure of  $\text{PW}_{12}\text{O}_{40}^{3-}$  unit remains intact. We noted that new absorption peaks at 3147 cm<sup>-1</sup>, 2958 cm<sup>-1</sup>, 1568 cm<sup>-1</sup> and 1165 cm<sup>-1</sup> appeared for the  $[\text{Bmim}]_3\text{PW}_{12}\text{O}_{40}$ ,  $\text{RuCl}_3/[\text{Bmim}]_3\text{PW}_{12}\text{O}_{40}$  and  $\text{Ru}/[\text{Bmim}]_3\text{PW}_{12}\text{O}_{40}$  samples, which can be assigned to the imidazole ring. The absorption peaks at 3147 cm<sup>-1</sup>, and 2958 cm<sup>-1</sup> were attributed to the C–H stretching mode of the imidazole ring and substituent group whereas the absorption peaks at 1568 cm<sup>-1</sup> and 1165 cm<sup>-1</sup> corresponded to the –C=N– and imidazole ring stretching mode [33].

### 3.2. Catalytic activity

#### 3.2.1. Catalytic conversion of microcrystalline cellulose

The  $\text{Ru}/[\text{Bmim}]_3\text{PW}_{12}\text{O}_{40}$  catalyst was tested in the conversion of microcrystalline cellulose and compared with the mixed  $[\text{Bmim}]_3\text{PW}_{12}\text{O}_{40} + \text{Ru/C}$  catalyst, as shown in Table 1. As a reference, we also run the reaction without adding any catalyst. Our

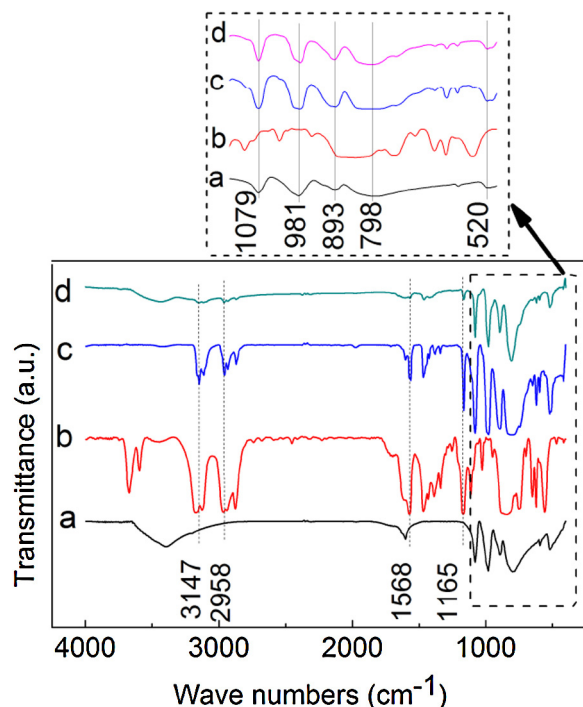


**Fig. 2.** FT-IR spectra of (a)  $\text{H}_3\text{PW}_{12}\text{O}_{40}$ , (b)  $[\text{Bmim}]_3\text{PF}_6$ , (c)  $[\text{Bmim}]_3\text{PW}_{12}\text{O}_{40}$ , and (d)  $\text{Ru}/[\text{Bmim}]_3\text{PW}_{12}\text{O}_{40}$ .

results showed that there was a small conversion of 6.6% after 10 h, attributed to the hydrolysis of cellulose at elevated temperature. In the presence of the  $[\text{Bmim}]_3\text{PW}_{12}\text{O}_{40} + \text{Ru/C}$  catalyst, the conversion of cellulose is increased to 35.5%, with oligosaccharide being the main product. There is no glucose formation with the  $[\text{Bmim}]_3\text{PW}_{12}\text{O}_{40} + \text{Ru/C}$  catalyst. In contrast, when the  $\text{Ru}/[\text{Bmim}]_3\text{PW}_{12}\text{O}_{40}$  catalyst was used, the conversion of cellulose was further improved to 42.6%. A more pronounced difference from that on the  $[\text{Bmim}]_3\text{PW}_{12}\text{O}_{40} + \text{Ru/C}$  catalyst is product distribution. The  $\text{Ru}/[\text{Bmim}]_3\text{PW}_{12}\text{O}_{40}$  catalyst exhibited a high selectivity toward sorbitol (58.0%). The selectivity of oligosaccharide is only 5.8%.

#### 3.2.2. Optimization of reaction conditions

After demonstrating that the  $\text{Ru}/[\text{Bmim}]_3\text{PW}_{12}\text{O}_{40}$  catalyst is highly selective toward sorbitol in the conversion of microcrystalline cellulose, we further optimized the reaction temperature and time to maximize the sorbitol yield, by changing the reaction temperature and controlling reaction time.

Fig. 3 shows cellulose conversion, sorbitol, glucose, and xylitol selectivity on the  $\text{Ru}/[\text{Bmim}]_3\text{PW}_{12}\text{O}_{40}$  catalyst at temperatures ranging from 393 K to 453 K and a reaction time of 10 h. Clearly, the conversion of cellulose increases as the reaction temperature

**Table 1**

Conversion of microcrystalline cellulose and selectivity of different products.

Catalyst	Conv. [%]	Selectivity [%]				
		Oli	Glu	Sor	Xyl	Gly
None <sup>a</sup>	6.6	90.0	0.6	–	–	–
$[\text{Bmim}]_3\text{PW}_{12}\text{O}_{40} + \text{Ru/C}$	35.5	52.6	–	4.5	9.6	1.0
$\text{Ru}/[\text{Bmim}]_3\text{PW}_{12}\text{O}_{40}$	42.6	5.8	7.9	58	6.8	0.3

Reaction conditions: cellulose, 0.25 g; 5 wt%  $\text{Ru}/[\text{Bmim}]_3\text{PW}_{12}\text{O}_{40}$ , 0.05 g;  $[\text{Bmim}]_3\text{PW}_{12}\text{O}_{40}$ , 0.05 g; 5 wt%  $\text{Ru/C}$ , 0.05 g; water 5 mL; 10 h; 433 K;  $\text{H}_2$ , 5 MPa.

<sup>a</sup> Ambient pressure; Oli = oligosaccharide; Glu = glucose; Sor = sorbitol; Xyl = xylitol; Gly = glycol; Meth = methanol.

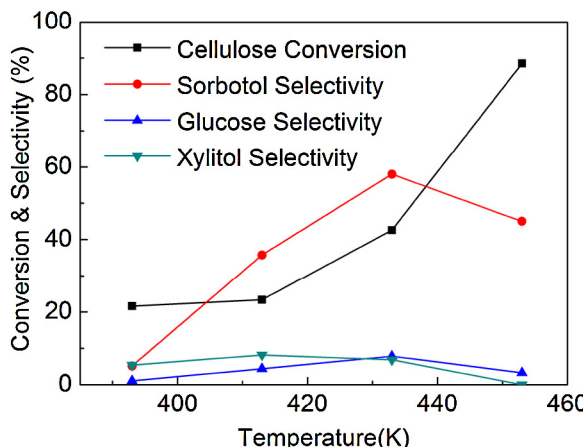


**Fig. 3.** Conversion of cellulose and selectivity for different products at different temperatures. Reaction conditions: cellulose, 0.25 g; 5 wt% Ru/[Bmim]<sub>3</sub>PW<sub>12</sub>O<sub>40</sub>, 0.05 g; water, 5 mL; H<sub>2</sub>, 5 MPa; reaction time, 10 h.

is increased. At 453 K, the conversion reaches 88.6%. On the other hand, the selectivity of sorbitol increases as the temperature is increased, reaching a maximum at ~433 K, and then decreases. Higher reaction temperatures degraded the product into anhydrous sorbitol (18.6%), erythrol (3.4%) and glycol (2.0%). Therefore, temperature has to be controlled at ~433 K to maximize the selectivity toward sorbitol although higher temperatures would result in a higher conversion of cellulose.

Reaction time is another parameter that can be controlled to optimize conversion and selectivity for a batch reaction. Fig. 4 shows the conversion of microcrystal cellulose and the selectivity toward the major products at 433 K with different reaction times. As shown in Fig. 4, the conversion of cellulose increases almost linearly with the reaction time. On the other hand, the selectivity toward sorbitol increases from 20.8% in 2 h to 70.3% in 24 h. Further increasing the reaction time to 36 h resulted in a sorbitol selectivity of 38.1%, significantly decreased from the maximum value. Consequently, degradation products including anhydrous sorbitol (16.1%), 5-HMF (12%), glucose (1.7%), erythrol (2.3%), glycol (1.3%) 1,2-propylene glycol (0.9%), levulinic acid (0.5%) and formaldehyde (8.0%) as well as a small amount of ethanol start to form.

### 3.3. Mechanism study

We chose cellobiose as a probe molecule to study the mechanism of the reactivity and selectivity of the Ru/[Bmim]<sub>3</sub>PW<sub>12</sub>O<sub>40</sub> catalyst. Fig. 5(a) and (b) compare the results of hydrogenolysis of cellobiose catalyzed by [Bmim]<sub>3</sub>PW<sub>12</sub>O<sub>40</sub> + Ru/C and

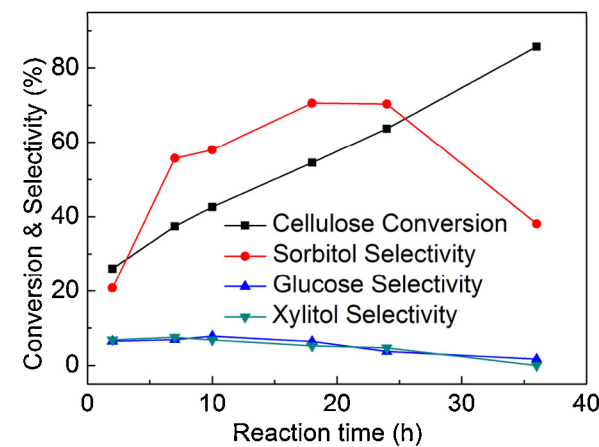


**Fig. 4.** Variation of cellulose conversion and selectivity for different products with reaction time at 433 K. Reaction conditions: cellulose, 0.25 g; 5 wt% Ru/[Bmim]<sub>3</sub>PW<sub>12</sub>O<sub>40</sub>, 0.05 g; water, 5 mL; H<sub>2</sub>, 5 MPa.

Ru/[Bmim]<sub>3</sub>PW<sub>12</sub>O<sub>40</sub>, respectively. As shown in Fig. 5, both catalysts convert cellobiose effectively, with conversion reaching almost 100% over [Bmim]<sub>3</sub>PW<sub>12</sub>O<sub>40</sub> + Ru/C and 76.8% over Ru/[Bmim]<sub>3</sub>PW<sub>12</sub>O<sub>40</sub> in 30 min. A rough estimate, by assuming a first-order reaction, shows that [Bmim]<sub>3</sub>PW<sub>12</sub>O<sub>40</sub> + Ru/C converts cellobiose almost 3 times faster than Ru/[Bmim]<sub>3</sub>PW<sub>12</sub>O<sub>40</sub>. However, the selectivity of the reaction with the two catalysts is in stark contrast: the main product over [Bmim]<sub>3</sub>PW<sub>12</sub>O<sub>40</sub> + Ru/C is glucitol (3-β-D-glucopyranosyl-D-glucitol, sugar alcohol of cellobiose), reaching a maximum value of 88.8% at 30 min and maintaining essentially constant over the reaction time whereas the selectivity toward sorbitol is low, reaching only 19.0% with a 3 h reaction time. On the other hand, both glucitol and glucose were formed with Ru/[Bmim]<sub>3</sub>PW<sub>12</sub>O<sub>40</sub> as the catalyst. The glucitol and glucose intermediates went through a maximum of ~28.0% at ~30 min and ~60 min, respectively, and were consumed almost completely with a 3 h reaction time. Accompanying the disappearance of the intermediates, the selectivity toward sorbitol increases and reaches almost 100% in 3 h. As shown in Fig. 5(b), the sorbitol yield reaches 98.0% with a 3 h reaction time. Clearly, the Ru/[Bmim]<sub>3</sub>PW<sub>12</sub>O<sub>40</sub> catalyst has a superior selectivity toward sorbitol.

On the basis of the experimental observation, we propose a reaction mechanism on the Ru/[Bmim]<sub>3</sub>PW<sub>12</sub>O<sub>40</sub> catalyst, as shown in Fig. 6.

According to this mechanism, cellobiose is first hydrogenated to glucitol by the dissociatively adsorbed hydrogen atoms generated on the metallic Ru sites. Glycosidic bonds of glucitol are then cleaved over the acid sites to produce glucose and sorbitol. The

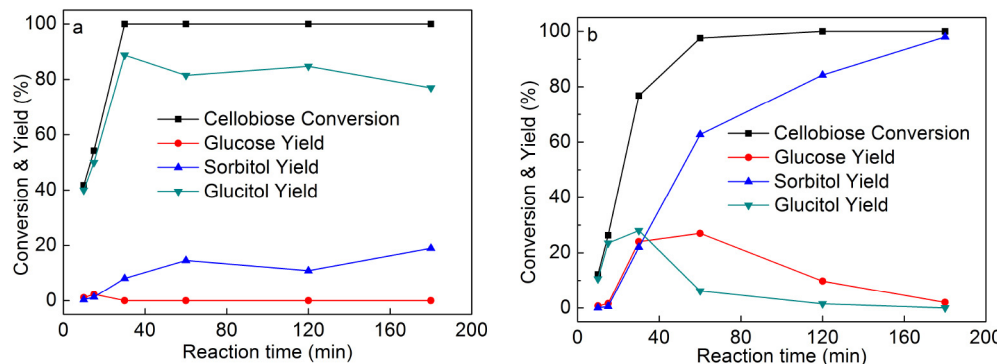


**Fig. 5.** Catalytic conversion of cellobiose under catalysts (a) [Bmim]<sub>3</sub>PW<sub>12</sub>O<sub>40</sub> + Ru/C, and (b) Ru/[Bmim]<sub>3</sub>PW<sub>12</sub>O<sub>40</sub>. Reaction conditions: cellobiose, 0.25 g; 5 wt% Ru/[Bmim]<sub>3</sub>PW<sub>12</sub>O<sub>40</sub>, 0.05 g; [Bmim]<sub>3</sub>PW<sub>12</sub>O<sub>40</sub>, 0.05 g; 5 wt% Ru/C, 0.05 g; water, 5 mL; 433 K; H<sub>2</sub>, 5 MPa.

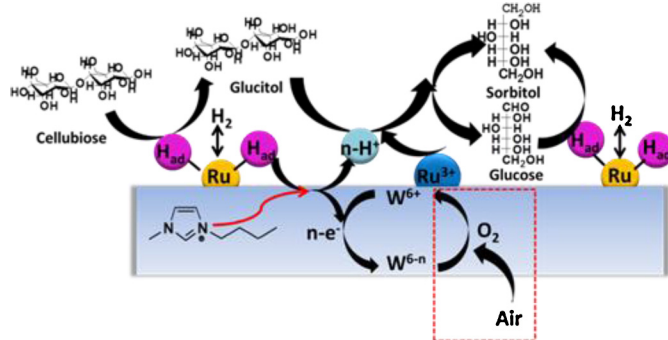


**Fig. 6.** Proposed mechanism of catalytic conversion of cellobiose into sorbitol.

glucose produced will be rapidly hydrogenated to sorbitol by the available hydrogen atoms on the metallic Ru sites. The proximity of the hydrogenation sites (metallic Ru sites) and the acid sites ( $W^{n+}$ ) on the Ru/[Bmim]<sub>3</sub>PW<sub>12</sub>O<sub>40</sub> catalyst is key to the observed superior selectivity. As shown in Fig. 5, the [Bmim]<sub>3</sub>PW<sub>12</sub>O<sub>40</sub> + Ru/C catalyst shows an even better hydrogenation activity, manifested by the high initial conversion rate of cellobiose. However, cellobiose is only hydrogenated to glucitol. The hydrolysis of glucitol was hindered by the lack of the immediately available acid sites. Consequently, glucitol is the main product of cellobiose hydrogenolysis catalyzed by the [Bmim]<sub>3</sub>PW<sub>12</sub>O<sub>40</sub> + Ru/C catalysts.

Hydrogen spillover is the main source of the Brønsted acid sites on Ru/[Bmim]<sub>3</sub>PW<sub>12</sub>O<sub>40</sub> catalyst [19]. The hydrogen adatom produced at the metallic Ru sites will likely spillover onto the O or W sites of the polyacids, generating protons and hydridic hydrogen, respectively, on the support. The protons can then migrate through [Bmim]<sup>+</sup> to the solution phase, making the reaction mixture acidic. We tested the hypothesis by measuring the pHs of reactant and product from the cellobiose hydrogenolysis at 433 K and 5 MPa H<sub>2</sub> for 3 h and summarized the results in Table 1. As shown in Table 2, the pHs are essentially unchanged before and after the reaction over the [Bmim]<sub>3</sub>PW<sub>12</sub>O<sub>40</sub> + Ru/C catalyst. In contrast, the pH was reduced from 4.4 to 2.5 after reaction over the Ru/[Bmim]<sub>3</sub>PW<sub>12</sub>O<sub>40</sub> catalyst. We exclude the contribution to the pH reduction from the acidic products, as HPLC analysis did not show any carboxylic acids in the product. In fact, the products of the cellobiose degradation are mainly sorbitol, with a small amount of glucose and glucitol. We also measured the pH changes of the solution containing only the catalysts (Ru/[Bmim]<sub>3</sub>PW<sub>12</sub>O<sub>40</sub> or [Bmim]<sub>3</sub>PW<sub>12</sub>O<sub>40</sub> + Ru/C) before and after the treatment in 5 MPa H<sub>2</sub> at 433 K for 3 h. The results, also shown in Table 2, indicate that similar pH changes to the reaction mixtures starting with cellobiose were achieved when the catalyst were treated in H<sub>2</sub> at the reaction conditions. Furthermore, the IR spectra of the liquid products of the cellobiose reaction, as shown in Fig. 7, further confirmed that there are no carboxyl characteristic peaks (~1700 cm<sup>-1</sup>) in the infrared spectra. The absorption peaks at 1415 cm<sup>-1</sup> was attributed to hydroxyl group of hexitols and those at 1650 cm<sup>-1</sup> and 3400 cm<sup>-1</sup> were assigned to adsorbed water. These results demonstrate that hydrogen spillover generates Brønsted acid sites formed during reaction over the Ru/[Bmim]<sub>3</sub>PW<sub>12</sub>O<sub>40</sub>

**Table 2**

The pH values of the reactive mixtures before and after the reaction at 433 K and 5 MPa H<sub>2</sub> for 3 h with different catalysts.

Catalyst		Initial	After reaction
Ru/[Bmim] <sub>3</sub> PW <sub>12</sub> O <sub>40</sub>	Catalyst only	4.4	2.5
	With cellobiose	4.4	2.4
[Bmim] <sub>3</sub> PW <sub>12</sub> O <sub>40</sub> + Ru/C	Catalyst only	4.6	4.4
	With cellobiose	4.6	4.4

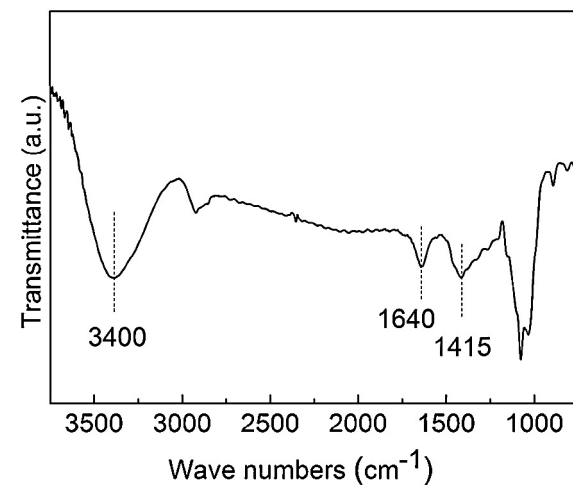


**Fig. 7.** FT-IR spectra of the liquid products of cellobiose transformations in 3 h at 433 K.

catalyst. The Ru/[Bmim]<sub>3</sub>PW<sub>12</sub>O<sub>40</sub> catalyst allowing a close contact between the Ru site and the O site, synergistically facilitates the hydrogenolysis reactions.

We used pyridine adsorption and FT-IR to characterize Brønsted acidity of the Ru/[Bmim]<sub>3</sub>PW<sub>12</sub>O<sub>40</sub> and [Bmim]<sub>3</sub>PW<sub>12</sub>O<sub>40</sub> + Ru/C catalysts and presented the results in Fig. 8. As shown in Fig. 8(a), the 1540 cm<sup>-1</sup> peak characterizing pyridine adsorption on the Brønsted sites is clearly seen after treating the Ru/[Bmim]<sub>3</sub>PW<sub>12</sub>O<sub>40</sub> catalyst in a H<sub>2</sub> + N<sub>2</sub> mixture. This peak was clearly a result of hydrogen treatment as there is no peak at this position in Fig. 8(b) when the catalyst was treated with only N<sub>2</sub>. Liu et al. have also demonstrated that hydrogen spillover was the source of Brønsted sites on the Ru/Cs<sub>3</sub>PW<sub>12</sub>O<sub>40</sub> catalyst [16]. These authors used pyridine-adsorbed FT-IR and confirmed the generation of the Brønsted sites due to hydrogen treatment. In our study, the 1540 cm<sup>-1</sup> peak was not observed in H<sub>2</sub> + N<sub>2</sub> treated [Bmim]<sub>3</sub>PW<sub>12</sub>O<sub>40</sub> + Ru/C, indicating that there is no Brønsted site generated on this catalyst. The inability of generating Brønsted sites on [Bmim]<sub>3</sub>PW<sub>12</sub>O<sub>40</sub> + Ru/C is because C can not act as an acceptor of the proton from H spillover. Furthermore, the spatial separation between the Ru sites and the O sites on the mixed catalyst prevented H to migrate to the O sites.

To determine the nature and role of the Ru species in Ru/[Bmim]<sub>3</sub>PW<sub>12</sub>O<sub>40</sub> catalyst, we performed a XPS analysis. Due

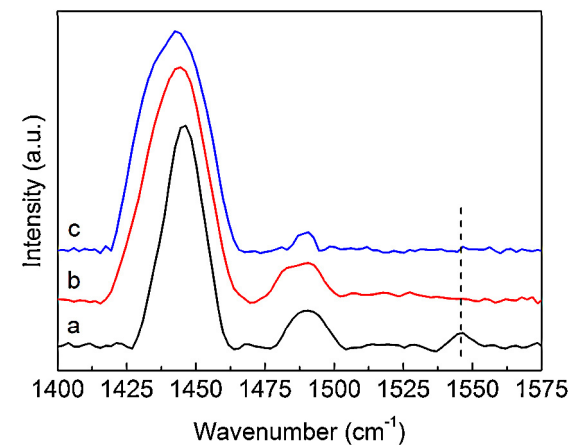


**Fig. 8.** Pyridine-adsorbed FT-IR spectra of (a) Ru/[Bmim]<sub>3</sub>PW<sub>12</sub>O<sub>40</sub> after treating in a H<sub>2</sub> + N<sub>2</sub> (10:90) mixture at ambient pressure and 473 K for 1 h, (b) Ru/[Bmim]<sub>3</sub>PW<sub>12</sub>O<sub>40</sub> after treating in N<sub>2</sub> at ambient pressure and 473 K for 1 h, (c) Ru/C+[Bmim]<sub>3</sub>PW<sub>12</sub>O<sub>40</sub> after treating in a H<sub>2</sub> + N<sub>2</sub> (10:90) mixture at ambient pressure and 473 K for 1 h.

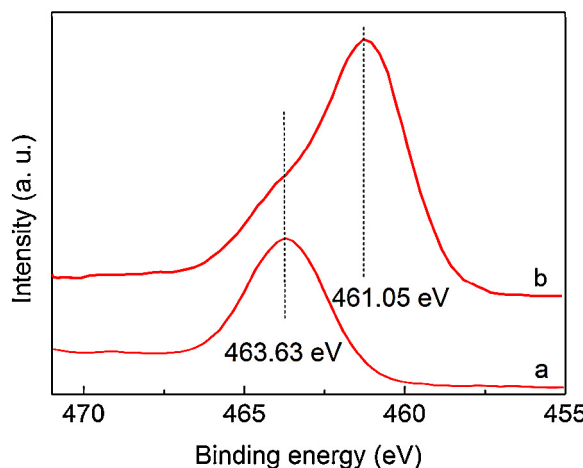


**Fig. 9.** Ru 3p<sub>3/2</sub> XPS spectra of (a) RuCl<sub>3</sub> and (b) Ru/[Bmim]<sub>3</sub>PW<sub>12</sub>O<sub>40</sub>.

to the fact that the binding energy of Ru 3d<sub>5/2</sub> orbital overlaps with that of C 1s, the Ru 3p<sub>3/2</sub> orbital was used in the analysis. As shown in Fig. 9, Ru 3p<sub>3/2</sub> in Ru/[Bmim]<sub>3</sub>PW<sub>12</sub>O<sub>40</sub> shows a broad peak centered at ~461.05 eV, corresponding to the metallic Ru (~76%). There is another weak peak at 463.63 eV, which was assigned to Ru(III) (~24%) by comparing with the spectrum from a reference RuCl<sub>3</sub> sample. The contribution from formation of RuO<sub>x</sub> during handling and preparation of the sample can be excluded as the Ru 3p<sub>3/2</sub> lines lie outside the range [34]. The results indicate that the Ru species on Ru/[Bmim]<sub>3</sub>PW<sub>12</sub>O<sub>40</sub> was not reduced completely to the metallic state, and therefore, Ru(III) coexists with the metallic state. Consequently, the Ru(III) sites with Lewis acidity are also likely to contribute to the hydrolysis activity toward cellulose on the Ru/[Bmim]<sub>3</sub>PW<sub>12</sub>O<sub>40</sub> catalyst. In summary, in addition to the Brønsted acidic sites generated from hydrogen spillover, the Lewis acidic active centers (Ru(III) and W<sup>5+</sup>) on the Ru/[Bmim]<sub>3</sub>PW<sub>12</sub>O<sub>40</sub> catalyst may also contribute to the observed hydrolysis activity.

Interestingly, we observed that the reaction mixture was dark blue immediately after the reaction over the Ru/[Bmim]<sub>3</sub>PW<sub>12</sub>O<sub>40</sub> catalyst, as shown in Fig. 10(a). After leaving the mixture in air overnight, white precipitates formed and the liquid mixture turned colorless, as shown in Fig. 10(b). The formation of solid precipitates and change of color correspond to the oxidation of the reduced W sites in air at room temperature formed during the hydrogenolysis helping the catalyst to regain its activity [35]. We incorporated this step in the dashed box of the mechanism shown in Fig. 6.

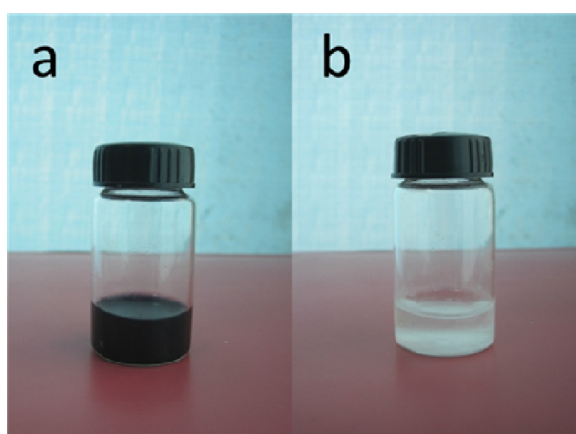


**Fig. 10.** Photographs of the liquid products (a) immediately after reaction and (b) after leaving overnight in air.

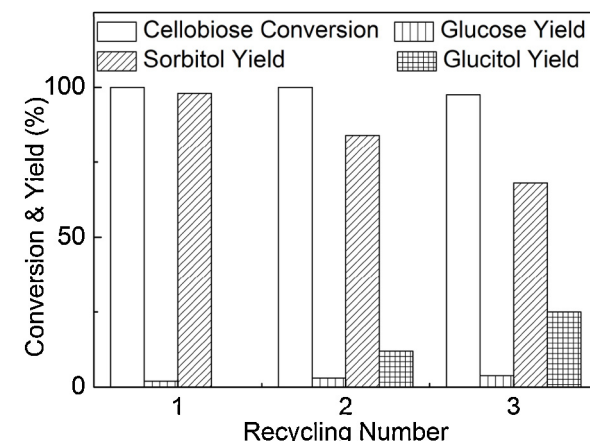


**Fig. 11.** Reusability of the catalyst for the conversion of cellobiose to sorbitol. Reaction conditions: cellobiose, 0.25 g; 5 wt% Ru/[Bmim]<sub>3</sub>PW<sub>12</sub>O<sub>40</sub>, 0.05 g; water, 5 mL; 433 K; H<sub>2</sub>, 5 MPa.

The formation of Brønsted acid active centers and the existence of Lewis acidic sites are in synergy with the metallic Ru sites, making the Ru/[Bmim]<sub>3</sub>PW<sub>12</sub>O<sub>40</sub> catalyst active and selective for hydrogenolysis of cellobiose to sorbitol. The same mechanism should be operative for the hydrogenolysis of cellulose on the Ru/[Bmim]<sub>3</sub>PW<sub>12</sub>O<sub>40</sub> catalyst, resulted in high selectivity to sorbitol.

#### 3.4. Reusability

The reusability of catalysts has been examined using the hydrogenolysis of cellobiose. After run of the reaction, the remaining solid were collected and centrifuged and washed with deionized water. The resulting solid was used as catalyst in the next run. Fig. 11 summarizes the results in the bar chart the conversion and yields of the reaction. Obviously, the conversion of cellobiose remained almost constant in the second and third run. However, the yield of sorbitol decreased significantly. Meanwhile, the glucitol yield was increased, reaching 25% in the third run. In order to understand the change of the selectivity in different runs, we analyzed the liquid products using the inductively coupled plasma (ICP). The results showed that 20 wt% of the W and 0.06 wt% of the Ru content (based on the fresh catalyst) were leached to liquid products. We speculate that the loss of more active W reduces the number of receiving site of spillover hydrogen, and thereby, the hydrolysis activity. Consequently, it becomes difficult to break up glycosidic linkages after cellobiose hydrogenation, resulting in the increased yield of glucitol.

#### 4. Conclusions

A catalyst consisting of supported Ru and an ionic liquid (BmimPF<sub>6</sub>)–Heteropoly acid (H<sub>3</sub>PW<sub>12</sub>O<sub>40</sub>·nH<sub>2</sub>O) hybrid as a support has been synthesized. The catalyst, with the Ru sites being in close contact with the oxygen sites of the support, facilitates hydrogen spillover and generates Brønsted acid sites in situ and acidifies the reactive mixture. On this catalyst, the Ru sites for hydrogenation combine with both Lewis and Brønsted acidic sites for hydrolysis, produced a synergy toward a superior catalytic performance for the selective conversion of microcrystalline cellulose to hexitols, resulted in a sorbitol selectivity of 70.3% with a microcrystalline cellulose conversion of 63.7% at 433 K with 5 MPa H<sub>2</sub> in 24 h. The proximity of the hydrogenation sites and the acid sites on the Ru/[Bmim]<sub>3</sub>PW<sub>12</sub>O<sub>40</sub> catalyst is key to the observed superior selectivity. The synergy between the IL–HPA hybrid and the

supported Ru was revealed through a mechanistic analysis: hydrogen spilled-over from the Ru site to the surface sites of the IL–HPA hybrid and its subsequent acidification of the reactive mixture via proton transfer through [Bmim]<sup>+</sup> played key roles in the enhanced catalytic performance.

## Acknowledgments

The work was supported by Nature Sciences Foundation of China (Grant No. 21076152 and No. 21276191), Special Research Fund for the Doctoral Program of Higher Education of China (Grant No. 2100032110018), and the Program of Introducing Talents of Discipline to Universities, China (Grant No. B06006).

## Appendix A. Supplementary data

Supplementary data associated with this article can be found, in the online version, at <http://dx.doi.org/10.1016/j.cattod.2013.09.061>.

## References

- [1] D.L. Klass, Biomass for renewable energy and fuels, in: J.C. Cutler (Ed.), Encyclopedia of Energy, Elsevier, New York, 2004, pp. 193–212.
- [2] A.M. Ruppert, K. Weinberg, R. Palkovits, *Angew. Chem. Int. Ed.* 51 (2012) 2564–2601.
- [3] D.M. Alonso, J.Q. Bond, J.A. Dumesic, *Green Chem.* 12 (2010) 1493–1513.
- [4] J.N. Chheda, G.W. Huber, J.A. Dumesic, *Angew. Chem. Int. Ed.* 46 (2007) 7164–7183.
- [5] A. Corma, S. Iborra, A. Velty, *Chem. Rev.* 107 (2007) 2411–2502.
- [6] W.P. Deng, Q.H. Zhang, Y. Wang, *Dalton Trans.* 41 (2012) 9817–9831.
- [7] C.H. Zhou, X. Xia, C.X. Lin, D.S. Tong, J. Beltramini, *Chem. Soc. Rev.* 40 (2011) 5588–5617.
- [8] S. Van De Vyver, J. Geboers, P.A. Jacobs, B.F. Sels, *ChemCatChem* 3 (2011) 82–94.
- [9] H. Kobayashi, H. Ohta, A. Fukuoka, *Catal. Sci. Technol.* 2 (2012) 869–883.
- [10] N. Yan, C. Zhao, C. Luo, P.J. Dyson, H.C. Liu, Y. Kou, *J. Am. Chem. Soc.* 128 (2006) 8714–8715.
- [11] A. Fukuoka, P.L. Dhepe, *Angew. Chem. Int. Ed.* 45 (2006) 5161–5163.
- [12] C. Luo, S.A. Wang, H.C. Liu, *Angew. Chem. Int. Ed.* 46 (2007) 7636–7639.
- [13] R. Palkovits, K. Tajvidi, A.M. Ruppert, J. Procelewska, *Chem. Commun.* 47 (2011) 576–578.
- [14] J. Geboers, S. Van de Vyver, K. Carpentier, K. de Blochouse, P. Jacobs, B. Sels, *Chem. Commun.* 46 (2010) 3577–3579.
- [15] J. Geboers, S. Van de Vyver, K. Carpentier, P. Jacobs, B. Sels, *Green Chem.* 13 (2011) 2167–2174.
- [16] M. Liu, W.P. Deng, Q.H. Zhang, Y.L. Wang, Y. Wang, *Chem. Commun.* 47 (2011) 9717–9719.
- [17] R.B. Levy, M. Boudart, *J. Catal.* 32 (1974) 304–314.
- [18] W.C. Conner, J.L. Falconer, *Chem. Rev.* 95 (1995) 759–788.
- [19] R. Prins, *Chem. Rev.* 112 (2012) 2714–2738.
- [20] R.P. Swatloski, S.K. Spear, J.D. Holbrey, R.D. Rogers, *J. Am. Chem. Soc.* 124 (2002) 4974–4975.
- [21] Z. Li, Q. Zhang, H. Liu, P. He, X. Xu, J. Li, *J. Power Sources* 158 (2006) 103–109.
- [22] A. Corma, S. Iborra, F. Xamena, R. Monton, J.J. Calvino, C. Prestipino, *J. Phys. Chem. C* 114 (2010) 8828–8836.
- [23] M. Ammam, J. Fransaer, *J. Electrochem. Soc.* 158 (2011) A14–A21.
- [24] Y. Leng, J. Wang, D.R. Zhu, X.Q. Ren, H.Q. Ge, L. Shen, *Angew. Chem. Int. Ed.* 48 (2009) 168–171.
- [25] Y. Leng, J. Wang, D.R. Zhu, Y.J. Wu, P.P. Zhao, *J. Mol. Catal. A: Chem.* 313 (2009) 1–6.
- [26] C.Z. Li, Z.K.B. Zhao, *Adv. Synth. Catal.* 349 (2007) 1847–1850.
- [27] H. Wang, G. Gurau, R.D. Rogers, *Chem. Soc. Rev.* 41 (2012) 1519–1537.
- [28] N. Yan, Y.A. Yuan, R. Dykeman, Y.A. Kou, P.J. Dyson, *Angew. Chem. Int. Ed.* 49 (2010) 5549–5553.
- [29] Y.S. Qu, C.P. Huang, J. Zhang, B.H. Chen, *Bioresour. Technol.* 106 (2012) 170–172.
- [30] Z. Sun, M.X. Cheng, H.C. Li, T. Shi, M.J. Yuan, X.H. Wang, Z.J. Jiang, *RSC Adv.* 2 (2012) 9058–9065.
- [31] M. Liu, H. Wang, J. Han, Y. Niu, *Carbohydr. Polym.* 89 (2012) 607–612.
- [32] C. Pazé, S. Bordiga, A. Zecchina, *Langmuir* 16 (2000) 8139–8144.
- [33] S. Yang, J.-z. Gui, D. Liu, X.-l. Peng, Y.-h. Gao, Y.-j. Zhang, *J. Petrochem. Univ.* 24 (2011) 31–39.
- [34] A.V. Naumkin, A. Kraut-Vass, S.W. Gaarenstroom, C.J. Powell, *NIST X-ray Photoelectron Spectroscopy Database*, in: NIST Standard Reference Database, vol. 20, National Institute of Standards and Technology, Gaithersburg, 2012.
- [35] Z.J. Tai, J.Y. Zhang, A.Q. Wang, M.Y. Zheng, T. Zhang, *Chem. Commun.* 48 (2012) 7052–7054.